Biotribology 20 (2019) 100109

Contents lists available at ScienceDirect

Biotribology

journal homepage: www.elsevier.com/locate/biotri

A method for eliminating the need to know when contact is made with soft surfaces: Data processing and error analysis

Marcus Garcia, Thomas E. Angelini*

Department of Mechanical and Aerospace Engineering, University of Florida, Gainesville, FL, USA

ARTICLE INFO

Keywords:
Error analysis
Hertz
Winkler
Soft matter
Indentation
Contact mechanics

ABSTRACT

The material properties of soft substances can be measured from bulk, homogeneous samples using rheometers and tensile testing instruments, while such characterization often requires indentation methods when sample preparation and geometry are highly constrained. For example, it is advantageous to use indentation instruments to measure the elastic moduli of living cells, confluent cell layers, tissue samples, hydrogel coatings, or soft objects with defined shapes and heterogeneous compositions like contact lenses. However, it is often exceedingly difficult to determine the point of contact between an indenting instrument and a soft sample. Here we describe a method that eliminates the need to determine the point of contact and we perform a thorough analysis of the errors associated with this analysis approach. The method involves averaging and differentiating experimental force-depth curves and reformulating classical contact mechanics models in terms of the applied force, F, and the first derivative of force with respect to indenter position, F'. Simulated indentation measurements of thick and thin hydrogel slabs with varying levels of noise and data averaging reveal that small errors are generated over a wide range of parameter space. Additionally, we provide a method for propagating errors from statistical variations in data to generate confidence intervals, facilitating the use of this data analysis method.

1. Introduction

Indentation methods have been used extensively to characterize the elastic moduli of hard materials like metals and ceramics [1–4]. Many of the mechanical models describing the contact forces between an indenter and a substrate can be reduced to power-law relationships of the form $F = Kd^P$, where F is the force, d is the depth of indentation, K contains material and system constants, and P is dependent on the geometry of the system [5–9]. More recently, indentation tests and contact models have been employed to investigate soft matter systems [10–14], including studies of hydrogels [15], cells [16,17] and cell layers [18,19]. However, a major limitation in most indentation measurements of soft systems is the difficulty of pin-pointing the point of contact, d_0, between a sample surface and indenter. A diversity of approaches have been taken to determine d_0, including optical measurements [20], regression algorithms [21], and successive search algorithms where every data point of the loading curve is treated as a potential point of contact [22,23]. An experimental two step indentation method was devised to determine the point of contact when speed-dependent effects contribute to the measurement [24]. Our previous work showed that small errors in d_0 can lead to enormous errors in estimated elastic moduli, even when a good fit to data is achieved [25]. To remedy this source of error, we developed a new analysis method to eliminate the need for determining the point of contact. Through a series of computer simulations and experimental indentations on polyacrylamide (pAAm) hydrogels the new method was shown to aid in the selection of the appropriate model which best described the sample and provided accurate measurements of the elastic modulus. However, no characterization of the error and uncertainty introduced with this new methodology has been developed. To provide confidence in this new method and facilitate its adoption by diverse researchers seeking to perform indentation measurements on soft systems, it is critical to investigate the errors and uncertainties it introduces.

Here we investigate the error and uncertainty associated with our new analysis method through a series of simulated indentation measurements of soft substrates that obey the Hertz and Winkler contact models. The analysis method involves binning noisy force-indentation curves, differentiating the binned data, then computing an elastic modulus. To systematically explore the dominating origins of error and uncertainty, we vary both the noise amplitude in force measurements and the size of data bins. We also perform a propagation of error analysis to predict an expected variance in elastic modulus calculations for a wide range of potential scenarios, comparing measured errors to theoretical uncertainties. A comparison between the two contact

* Corresponding author.
E-mail address: t.e.angelini@ufl.edu (T.E. Angelini).

https://doi.org/10.1016/j.biotri.2019.100109
Received 26 February 2019; Received in revised form 4 September 2019; Accepted 22 September 2019
Available online 31 October 2019

models shows that our analysis method produces more error for data following the Winkler model, yet errors are generally low; the 99.7% confidence intervals of elastic moduli measured from data following either model fall within 7% of the true value. Additionally, over a wide range of parameter space of varying data bin size and measured noise amplitude, we find < 3% error in measured elastic moduli, relative to the known value.

2. Methods

2.1. Summary of previously reported experiments

The loading curves simulated and analyzed in this manuscript are based on experiments from our previous work [25]. Here we provide a brief overview of these experimental details to motivate the specific details included in the simulations described in this manuscript. Polyacrylamide (pAAm) hydrogel samples were made at 7.5% polymer concentration and different sample thicknesses. The hydrogel sheets were prepared using the protocols reported in Urueña et al. [28] and allowed to equilibrate in ultrapure water (18.2 MΩ) for 24 h. The sample thicknesses were controlled during polymerization by casting the hydrogels between two 22 × 22 mm^2 glass cover slips separated by 100 μm and 1000 μm thick spacers. The top coverslips were removed before indentation either spontaneously through the swelling process or by gentle mechanical agitation.

Indentation was performed near the centers of the hydrogel samples to minimize possible edge effects. The hydrogel samples were submerged in ultrapure water and indented with a piezo-driven, quasistatic transducer indentation system (Hysitron BioSoft) with a hemispherical indenter tip, also submerged in the water bath. The indentation tip was a borosilicate glass hemisphere (R = 1 mm), which was plasma cleaned and coated with F-127 Pluronic between each experiment to reduce adhesion to the hydrogel surfaces. In these experiments, the indenter begins at some unknown distance from the surface, d_0, approaches the surface monotonically, touches the surface, and indents at a constant piezo displacement rate of 10 nm/s for 100 μm thick specimens and 1 μm/s for 1000 μm thick specimens. The samples were loaded by moving the piezo stage to specified locations in a displacement-controlled operation mode. Force-response and positions were measured simultaneously by the quasistatic transducer at a rate of 125 Hz. In this displacement-controlled mode, the primary source of noise was found to be in the force-signal; measured indentation depths were found to be very smooth in time. Thus, in this work we focus entirely on noise originating from force measurements. In future work it will be interesting to explore force-controlled experiments in which the dominating origin of noise arises from feeding back on force measurements while constantly adjusting the indenter position. We believe the method described here could be re-formulated to smooth out noisy position measurements rather than noisy force measurements, or possibly smoothing both potentially noisy signals.

2.2. Overview of the analysis method

Force-indentation curves using a variety of probe geometries are well-described by simple power law relationships, which can be used to characterize soft materials. Among these are the flat-ended cylindrical punch and indenters with conical, hemispherical, paraboloid shapes [9]. For hemispherical indenters, the Hertz and Winkler contact models are often used to analyze loading curves produced by applying a force, F, to the surface of a material that indents by a distance, u, at the apex of an indenting instrument. While contact models are often generalized to described interfaces between surfaces with two different curvatures made from materials with two different material properties, we focus here on infinitely stiff, hemispherical indenting instruments pressing against flat, soft substrates. However, we note that the method can be modified to analyze measurements for which any two contacting geometries produce force-displacement curves that obey a power law scaling relationship. When using a hemispherical indenter to test slabs of material much thicker than the width of the interface under contact, the Hertz [26] contact model is used, which has an F-u relationship given by

$$F = \frac{4}{3}E^*R^{1/2}(u - d_0)^{3/2} \equiv K_H d^{3/2}, \tag{1}$$

where F is applied force, E^* is the modulus of elasticity of the material, R is the radius of curvature of the indenter probe, u is the indenter location, d_0 is the location of the surface at which the indenter first makes contact, $d = u - d_0$ is the indentation depth, and K_H is a pre-factor for writing the relation compactly. When using a hemispherical indenter to test thin slabs of material where the contact width is larger than the substrate thickness, the Winkler [27] contact model is used, which has an F-u relationship given by

$$F = \frac{\pi E^* R}{h}(u - d_0)^2 \equiv K_W d^2, \tag{2}$$

where the parameters are the same as in the Hertz model except for the addition of h, the slab thickness, and K_W a pre-factor for writing the relation more compactly. To perform experiments for determining E^*, any general power law that relates F to u usually requires knowledge of d_0 either ahead of time or through additional experimental or analysis approaches. To eliminate the need to know d_0, the F-u power law can be differentiated with respect to u, $F' = dF/du$, and the original F-u relationship can be used to eliminate u-d_0. For any power-law contact model, $F = Kd^P$, the resulting relation is given by

$$F' = K_G F^n, \tag{3}$$

where $K_G = PK^{1/P}$ is a generalized coefficient and $n = (P - 1)/P$. K can be K_H, K_W or the coefficient of any F-u power-law relationship. For the Hertz model, $P = 3/2$ and $n = 1/3$; for the Winkler model, $P = 2$ and $n = 1/2$. For the Hertz model, following this procedure and solving for the elastic modulus results in a relationship given by

$$E^* = \frac{3}{4}\left(\frac{F'^{3/2}}{1.83R^{1/2}F^{1/2}}\right), \tag{4}$$

where the value 1.83 is approximately P^P with $P = 1.5$. The same procedure for the Winkler model produces a relationship for the elastic modulus given by

$$E^* = \frac{hF'^2}{4\pi RF}. \tag{5}$$

Using these relationships, measured F-u curves can be converted into local, point-by-point moduli, and averaged. Below we describe a procedure for computing F' from experimental and simulated data.

2.3. Implementation using experimental or simulated data

In the micro-indentation measurements simulated here, measurements of indenter position, u, are typically smooth, while simultaneous measurements of applied force, F, are often the dominant source of noise in F-u curves [25]. Thus, differentiating F-u curves requires some form of smoothing. To overcome this frequently encountered challenge in differentiating experimental data, we average F-u data falling within equally spaced force bins. This process requires re-casting the formulas derived above into forms that account for the binning process. Representative values of force, $\overline{F}_i$, and displacement, $\overline{u}_i$, within the i^{th} bin are found by computing the mean of all values falling within a specified force range. Performing a discrete derivative on this binned data, $\overline{F}_i'$ is given by

$$\overline{F}_i' = \frac{\overline{F}_{i+1} - \overline{F}_i}{\overline{u}_{i+1} - \overline{u}_i}, \tag{6}$$

where $\overline{F}_i$ and $\overline{F}_{i+1}$ are average forces of sequential bins along the loading

curve. Similarly, $\overline{u}_i$ and $\overline{u}_{i+1}$ are average indenter positions of the sequential bins. The force corresponding to each $\overline{F}_i'$ is chosen to be the mid-point between each successive pair of evenly spaced bins, given by

$$\overline{\overline{F}}_i = \frac{\overline{F}_{i+1} + \overline{F}_i}{2}. \tag{7}$$

The power law models for determining the elastic moduli are then recast in terms of indexed averaged variables. For the Hertz model, the modulus determined from each new bin is given by

$$E_i^* = \frac{3}{4}\left(\frac{\overline{F}_i'^{3/2}}{1.83R^{1/2}\overline{\overline{F}}_i^{1/2}}\right) \tag{8}$$

Similarly, the modulus for the Winkler contact model is given by

$$E_i^* = \frac{h\overline{F}_i'^2}{4\pi R\overline{\overline{F}}_i}. \tag{9}$$

The index on the elastic modulus for both models indicates that a value for the elastic modulus can be calculated for each point along the loading curve.

2.4. Propagation of error analysis

With the algebraic formulas developed above, it is straight-forward to propagate variations of $\overline{F}_i$ and $\overline{F}_i'$ within each bin to the corresponding calculation of E_i^*. The standard deviation of E_i^* is found from a generalized relation for variance given by

$$\sigma_z^2 \approx \sum_{i=1}^{p}\sum_{j=1}^{p}\left(\frac{\partial z}{\partial x_i}\right)\left(\frac{\partial z}{\partial x_j}\right)\sigma_{i,j}, \tag{10}$$

where z is the variable of interest and we approximate cross terms to be zero. Following this procedure for the case of the Hertz contact model, the standard deviation of E_i^* is given by

$$\sigma_{E_i^*} = E_i^*\sqrt{\left(\frac{9}{4\overline{F}_i'^2}\right)\sigma_{\overline{F}_i'}^2 + \left(\frac{1}{4\overline{\overline{F}}_i^2}\right)\sigma_{\overline{\overline{F}}_i}^2}, \tag{11}$$

where $\sigma_{\overline{F}_i'}^2$ is the variance of $\overline{F}_i'$, $\sigma_{\overline{\overline{F}}_i}^2$ is the variance in $\overline{\overline{F}}_i$ and $\sigma_{E_i^*}$ is the standard deviation in E^*, each for the i^{th} bin. The variances for $\overline{F}_i'$ and $\overline{\overline{F}}_i$ are found to be given by

$$\begin{aligned}\sigma_{\overline{F}_i'}^2 &= \left(\frac{1}{\overline{u}_{i+1}-\overline{u}_i}\right)^2\sigma_{\overline{F}_{i+1}}{}^2 + \left(\frac{1}{\overline{u}_{i+1}-\overline{u}_i}\right)^2\sigma_{\overline{F}_i}{}^2 + \left(\frac{\overline{F}_{i+1}-\overline{F}_i}{(\overline{u}_{i+1}-\overline{u}_i)^2}\right)^2 \\ &\quad \sigma_{\overline{u}_{i+1}}{}^2 + \left(\frac{\overline{F}_{i+1}-\overline{F}_i}{(\overline{u}_{i+1}-\overline{u}_i)^2}\right)^2\sigma_{\overline{u}_i}{}^2\end{aligned} \tag{12}$$

$$\sigma_{\overline{\overline{F}}_i}^2 = \frac{1}{4}(\sigma_{\overline{F}_{i+1}}^2 + \sigma_{\overline{F}_i}^2) \tag{13}$$

$\sigma_{\overline{F}_i}^2$, $\sigma_{\overline{F}_{i+1}}^2$, $\sigma_{\overline{u}_i}^2$, and $\sigma_{\overline{u}_{i+1}}^2$ are calculated for each bin. Similarly, the standard deviation, σ_{E^*}, of E^* for the case of the Winkler contact model is given by

$$\sigma_{E_i^*} = E_i^*\sqrt{\left(\frac{4}{\overline{F}_i'^2}\right)\sigma_{\overline{F}_i'}^2 + \left(\frac{1}{\overline{\overline{F}}_i^2}\right)\sigma_{\overline{\overline{F}}_i}^2}. \tag{14}$$

In both cases, the variances of R and h are treated as negligible compared to $\overline{F}'$ and $\overline{F}$, and are approximated as zero.

3. Results and discussion

3.1. Errors introduced by binning force measurements

Since force scales nonlinearly with displacement in the power law relationships investigated here, we expect the binning procedure described above to generate errors that vary systematically with the measured values. To investigate binning errors, we compute the difference between the averaged value of force in the i^{th} bin, $\overline{F}_i$, and the known value at the bin's midpoint. We perform this residual calculation along a simulated force-displacement curve that models experimental indents on soft substrates reported previously [25]. The experiments we model here used a hemispherical indenter of radius $R = 1$ mm and a polyacrylamide (pAAm) hydrogel substrate having an elastic modulus $E^* = 23.6$ kPa which was measured experimentally in our previous work by micro-indentation, and compared to bulk shear measurements (Fig. 1) [25]. To create finely spaced data-points to average over, we compute F at approximately 2×10^6 locations and place them in equally spaced force-bins, incremented by ΔF. We simulate an indent of a thin slab having thickness $h = 100\,\mu$m using the Winkler model; a thick slab ($h \gg 100\,\mu$m) is simulated using the Hertz model. To isolate errors arising solely from binning data, no noise is added to the simulations for the residual calculation, though both simulations are bounded at the low end by a noise floor of 5 μN to reproduce the lower force-limit reported in experiments. At the high-force end, we bound the simulations by an indentation depth of 20 μm, also mimicking the experiments (Fig. 1).

hydrogel material	7.5% (w/w) pAAm	7.5% (w/w) pAAm
model	Winkler $h < 2a$	Hertz $h >> 2a$
P	2	3/2
k	$\frac{\pi E^* R}{h}$	$\frac{4}{3}E^* R^{1/2}$
sample thickness, h	100μm	———
modulus, E	23.6 kPa	23.6 kPa
force range, F	5μN - 285μN	5μN - 90μN
depth range, u	2.6 - 20.0 μm	2.9 - 20.0 μm
max strain, $\gamma_{max} \leq 20\%$	$\gamma_{max} = \frac{u_{max}}{h} = 0.2$	$\gamma_{max} = \frac{u_{max}}{a} = 0.14$

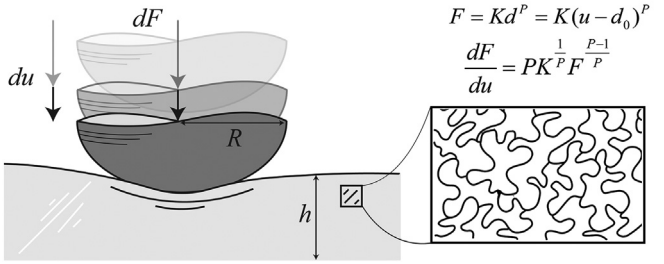

Fig. 1. Indentation measurements of thin and thick hydrogel substrates are simulated using the Winkler and Hertz contact models. The elastic modulus is calculated from F'-F curves and its residual is determined, enabling the quantification of error associated with the new method.

In the thick-slab simulation, we choose a bin-size of 2 μN, which represents a fairly coarse binning considering the largest force simulated is approximately 90 μN. The binned data appears to lay right on top of the smooth Hertz model curve (Fig. 2a). Indeed, a point-by-point calculation of the residual, $F_i - \overline{F}_i$, shows that the difference is always $< 10^{-2}$ μN; the binning error is never $> 0.33\%$, and is highest at low forces. The scaling relationship between this residual error and indenter position, u, turns out to be $u^{-3/2}$, the reciprocal of the Hertz power law (Fig. 2b). A similar analysis of the F' versus F data shows that the binned data points lay very close to the analytical model and that the residual error is never $> 0.33\%$. The scaling relationship between the residual error of F' and the applied force turns out to be $F^{-1.68}$ (Fig. 2c,d).

In the thin-slab simulation we explore the same range of indentation depth tested in the thick slab case, resulting in a maximum force of

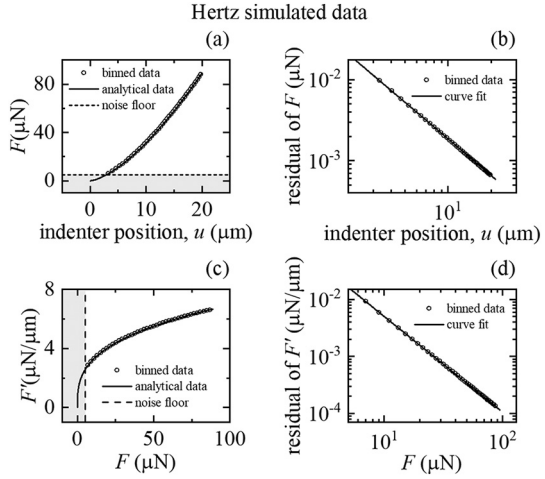

Fig. 2. To isolate the error produced from binning data, simulations of the Hertz model are run with no noise and data-points are binned using a bin size of 2 μN. The residuals of the binned data are found by comparing binned values to the values obtained from the Hertz model at the bin mid-points. The residual of F falls with a power of -1.5 with an R^2 of 0.9999 while the residual of F' decreases with a power of -1.682 ± 0.001 with an R^2 of 0.999.

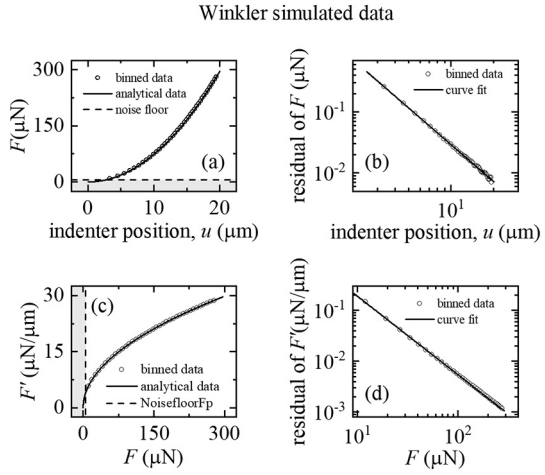

Fig. 3. Theoretical loading curves based on the Winkler model were also simulated with no noise to understand effects the power law has on error produced by binned data using a binsize of 7 μN. The residual of F falls with a power of -1.995 ± 0.003 with an R^2 of 0.9999 while the residual of F' falls with a power of -1.575 ± 0.006 with an R^2 of 0.9997.

approximately 285 μN; we choose a correspondingly larger bin width of 7 μN. The binned data points lay very close to the smooth Winkler model curve and the point-by-point residual, $F_i - \overline{F_i}$, exhibits an error that is always < 3.1% (Fig. 3a,b). In this case, the scaling relationship between this residual error and indenter position, u, turns out to be u^{-2}, the reciprocal of the Winkler power law (Fig. 3b). Applying this analysis approach to the F' versus F data also shows little difference between the binned data points and the analytical model; the residual error is never > 2.5%. The scaling relationship between the residual error of F' and the applied force is found to be $F^{-1.57}$ (Fig. 3c,d). While this analysis reveals that binning errors are larger for analysis of indentation data from thin slabs than from thick slabs, the errors are generally small for both thick and thin substrates. Binning errors in thin-slab measurements are larger than those in thick-slab measurements most likely because of the corresponding disparity in force-level at the same indentation depth, related to the stronger power of the Winkler scaling law ($P = 2$) relative to the Hertz scaling law ($P = 3/2$). In both cases, binning errors are found to be the largest at the lowest applied loads

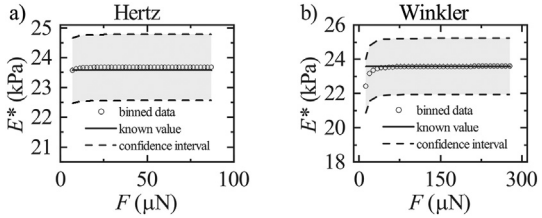

Fig. 4. We compute E^* as a function of applied force, F, using the (a) Hertz and (b) Winkler contact models with no noise to isolate the effects of data binning. Dashed lines are confidence intervals based on a propagation of uncertainty analysis using a 99.7% confidence. The known value of E^* (solid line) falls within the confidence interval of the calculated values of E^*. We note that in the Winkler contact model case, a relatively large error occurs for the first few bins when calculating elastic modulus.

and indentation depths, where the derivatives of the F-u curves are small.

To provide a priori estimates of uncertainty in measurements of E^* using our method, confidence intervals can be computed by propagating variations in F and F' through calculations of E^*, following the procedure described above in the Methods section. Accordingly, using Eqs. (8) and (9), we compute E^* from each of the simulated F'-F curves shown in Figs. 2 and 3. Comparing the values determined from simulated data to the known value that is put into the simulations we find that a well-defined value of E^* can be determined by averaging over most computed values. Plots of E^* versus F show that elastic modulus measurements agree very well with the known value over nearly the entire range of forces simulated (Fig. 4a,b). We also find that the E^* computed from the lowest two or three force bins are clear outliers, so we use the median of E^* as our representative value. The appearance of these outliers and their relative magnitudes across the Hertz and Winkler cases are consistent with our observations, above, that errors are highest at low forces and larger for thin-slab indents. Thus, as a general guideline, it is useful to compute E^* from median calculations rather than from means, reducing the influence of these few outliers. For the individual estimates of E^* computed for each averaged pair of F and F', the confidence interval, CI, is given by

$$CI = \pm 3\frac{\sigma_{E^*}}{\sqrt{N}}, \tag{15}$$

where N is the number of points in a bin and the factor of three corresponds to three standard deviations (99.7% confidence for Gaussian random variables). For the thick slab, we find an average CI of ± 1.2 kPa, and for the thin slab, we find $CI =$ ± 1.6 kPa. An important practical feature of CI is that it will determine the minimum sampling rate necessary for a desired confidence interval; an increased confidence can be achieved by increasing the number of samples within each force bin interval.

3.2. Combined noise and binning errors introduced in determining E^*

In the error calculations described above we chose a single bin-size in processing each of the simulated force curves to mimic data analysis of typical experiments. Additionally, no noise was added for the purpose of isolating potential errors introduced by our binning procedure. To gain insight into how these confounding variables may affect experimental measurements together, we perform additional simulations in which the force bin-size and measurement noise are systematically varied. To generate noisy F-u curves, uniformly distributed random numbers within a range ± ΔF are added to data points generated by the theoretical models, and a noise floor of $2\Delta F$ is chosen for each simulation. From these noisy F-u curves with varying bin-size, maps of E^* are generated using Eqs. (8) and (9) as described above. These averaged estimates of E^* are computed for all combinations of ΔF and bin-sizes tested; for the thick slab indent simulated from the Hertz model, ΔF and

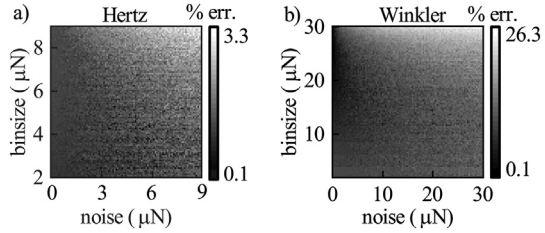

Fig. 5. We perform a series of simulations to characterize the error in our method for a variety of noise levels that may occur for different indentation measurements. Heat maps for (a) Hertz and (b) Winkler models show the residual in calculated elastic modulus for a range of noise levels and force bin sizes (shown on a logarithmic intensity scale to aid in visualizing trends). Fluctuations in residuals of point to point values for elastic modulus are comparable to local values producing a grainy heat map. Both heatmaps reveal growing errors with higher noise levels and larger bin sizes.

bin-size are varied between 2 μN and approximately 9 μN; for the thin slab indent simulated by the Winkler model, ΔF and bin-size are varied between 2 and 30 μN. In both cases, the upper limits of ΔF and bin-size are chosen to be roughly 1/10 the maximum applied force in the simulated *F-u* curves. The lower limits are chosen to reflect the typical noise-floor of micro-indentation instruments.

In the 2D maps of percent error in E^*, relative to the true value of 23.6 kPa, we find that the error dramatically rises near the largest levels of noise and largest bin-sizes; for most of the parameter space explored here the errors are so small that the 2D error maps must be displayed on a logarithmic scale in order to visualize the overall trends. Throughout the lower ranges of ΔF and bin-size, the random variations from point-to-point are comparable to the neighborhood values, creating a grainy error map (Fig. 5a,b). Consistent with the residual analysis of *F-u* and *F′-F* curves described in the previous section, the errors in analyzing thick slabs are generally less than those of thin slabs; the largest error found is approximately 3.3% for the thick slab case and 26.3% for the thin slab case. Apart from these maximal errors occurring at the largest noise levels and bin-sizes, the measured errors throughout most the remaining parameter space are < 3% for both the thick and thin slab cases and do not exhibit a strong dependence on bin-size. These low levels of error are found even in when the noise amplitude is much larger than the bin-size; we find that the smoothing of noise is largely controlled by the number of data-points in a bin, rather than the bin-size alone. While this analysis does not lead us to specific guidelines for analyzing data collected from the diversity of instruments most often used to perform indentation measurements, we hope the analysis shown here provides confidence that low levels of error are achievable when analyzing data having a wide range of different levels of noise.

4. Conclusions

In the work described here, we investigate errors in determining elastic moduli when using our recently developed analysis method that eliminates the need to know the point of contact in indentation measurements. This method involves discrete derivatives of experimental data; we hope that determining the errors produced by differentiating experimentally measured nonlinear loading curves will provide confidence to researches who wish to adopt the method. We therefore derived a formula for predicting confidence intervals of elastic moduli measurements, specific to our analysis method. We find that the measured residuals of elastic moduli are smaller than the theoretical confidence intervals, which is a result of how well linear approximations made by binned data reflect the original loading curves. Moreover, we find the residuals produced by binning ideal noise-free data to be negligible, and the method produces highly accurate elastic moduli when analyzing data with a wide range of noise levels and when averaging data using a wide range of bin sizes.

We limited our modeling in this investigation to one material system: a 7.5% pAAm hydrogel, having an elastic modulus of 23.6 kPa. This hydrogel represents a soft material in the middle-range one might encounter in biotribological systems – most soft tissues have elastic moduli in the 10 kPa range, while brain tissue is comparatively softer and cartilage is stiffer. Our results indicate that our analysis method is capable of measuring moduli across the range spanned by these tissues; our previous work showed the effectiveness of this method in measuring the elastic moduli of much softer gels having moduli of 4–6 kPa, and noise rapidly becomes negligible compared to measured force levels when measuring much stiffer materials.

The analysis method and error characterization described here are not restricted to micro-indentation techniques; data collected using many different kinds of indentation instrument can be processed with our method. Measurements of soft materials using macro-, micro-, and nano-indentation systems may benefit from this analysis method. For example, while atomic force microscopes (AFMs) fitted with colloidal-scale indenting probes have force and displacement resolutions of fractions of nano-Newtons and nanometers, the noise present in these measurements creates challenges with interpreting data near the point of contact [29]. Thus, even with high resolution in force and displacement and low levels of noise, uncertainty in the point of contact still exists. Thus, we expect our analysis method to help in such cases. However, challenges remain when using our method; in situations where the indenter detects forces as it moves toward a sample surface, force-offsets can be produced near the point of contact [24]. These forces can arise from the resistance generated by fluid “squeeze-out” at the interface between an indenter and a sample. The same deficiency in our method will arise when adhesive “snap-on” forces generate an uncontrolled offset in measured force; while our method eliminates the need to know the point of contact, it is not capable of eliminating the role of force-offsets. In such cases, our method could potentially be applied to a portion of the unloading-side of the force-displacement curve where elastic forces dominate. We are currently exploring the effects of offsets in force on elastic modulus measurements and developing new methods to eliminate their effects.

Acknowledgements

This work was supported by Alcon Laboratories.

Declaration of competing interest

We also affirm that all authors listed contributed significantly to the project and manuscript. Furthermore we confirm that none of our authors have disclosures and we declare no conflict of interest.

References

[1] R.W. Carpick, M. Salmeron, Scratching the surface: fundamental investigations of tribology with atomic force microscopy, Chem. Rev. 97 (1997) 1163–1194, https://doi.org/10.1021/cr960068q.
[2] A.C. Fischer-Cripps, Critical review of analysis and interpretation of nanoindentation test data, Surf. Coat. Technol. 200 (14–15) (2006) 4153–4165, https://doi.org/10.1016/j.surfcoat.2005.03.018.
[3] W.C. Oliver, G.M. Pharr, An improved technique for determining hardness and elastic modulus using load and displacement sensing indentation experiments, J. Mater. Res. 7 (6) (1992) 1564–1583, https://doi.org/10.1557/JMR.1992.1564.
[4] D. Tabor, Surface forces and surface interactions, J. Colloid Interface Sci. 58 (1) (1977) 2–13, https://doi.org/10.1016/0021-9797(77)90366-6.
[5] B.V. Derjaguin, V.M. Muller, Y.P. Toporov, Effect of contact deformations on the adhesion of particles, J. Colloid Interface Sci. 53 (2) (1975) 314–326, https://doi.org/10.1016/0021-9797(75)90018-1.
[6] H. H, On the contact of elastic solids, J Reine Angew Math 92 (1881) 156–171.
[7] K.L. Johnson, Contact Mechanics, Cambridge University Press, New York (NY), 1985.
[8] K.L. Johnson, K. Kendall, A.D. Roberts, Surface energy and the contact of elastic solids, Proc. R. Soc. Lond. A 324 (1971) 301–313, https://doi.org/10.1098/rspa.1971.0141.
[9] I.N. Sneddon, The relation between load and penetration in the axisymmetric Boussinesq problem for a punch of arbitrary profile, Int. J. Engng. Sci. 3 (1) (1965)

47–57, https://doi.org/10.1016/0020-7225(65)90019-4.
[10] E.P. Chan, Y. Hu, P.M. Johnson, Z. Suo, C.M. Stafford, Spherical indentation testing of poroelastic relaxations in thin hydrogel layers, Soft Matter 8 (2012) 1492–1498, https://doi.org/10.1039/C1SM06514A.
[11] J. Erath, S. Stephan, A. Fery, Characterization of adhesion phenomena and contact of surfaces by soft colloidal probe AFM, Soft Matter 6 (7) (2010) 1432–1437, https://doi.org/10.1039/B923540J.
[12] Y. Hu, X. Zhao, J.J. Vlassak, Z. Suo, Using indentation to characterize the poroelasticity of gels, Appl. Phys. Lett. 96 (2010) 121904, , https://doi.org/10.1063/1.3370354.
[13] P.C. Nalam, N.N. Gosvami, M.A. Caporizzo, R.J. Composto, R.W. Carpick, Nano-rheology of hydrogels using direct drive force modulation atomic force microscopy, Soft Matter 11 (2015) 8165–8178, https://doi.org/10.1039/C5SM01143D.
[14] K.D. Schulze, S.M. Hart, S.L. Marshall, C.S. O'Bryan, J.M. Uruena, A.A. Pitenis, W.G. Sawyer, T.E. Angelini, Polymer osmotic pressure in hydrogel contact mechanics, Biotribology 11 (2017) 3–7, https://doi.org/10.1016/j.biotri.2017.03.004.
[15] M.L. Oyen, Mechanical characterisation of hydrogel materials, Int. Mater. Rev. 59 (1) (2014) 44–59, https://doi.org/10.1179/1743280413Y.0000000022.
[16] R.E. Mahaffy, C.K. Shih, F.C. Mackintosh, J. Kas, Scanning probe-based frequency-dependent microrheology of polymer gels and biological cells, Phys. Rev. Lett. 85 (4) (2000) 880–883, https://doi.org/10.1103/PhysRevLett.85.880.
[17] S. Sen, S. Subramanian, D.E. Discher, Indentation and adhesive probing of a cell membrane with AFM: theoretical model and experiments, Biophys. J. 89 (5) (2005) 3203–3213, https://doi.org/10.1529/biophysj.105.063826.
[18] K.D. Schulze, S.M. Zehnder, J.M. Uruena, T. Bhattacharjee, W.G. Sawyer, T.E. Angelini, Elastic modulus and hydraulic permeability of MDCK monolayers, J. Biomech. 53 (2017) 210–213, https://doi.org/10.1016/j.jbiomech.2017.01.016.
[19] S.M. Zehnder, M.K. Wiatt, J.M. Uruena, A.C. Dunn, W.G. Sawyer, T.E. Angelini, Multicellular density fluctuations in epithelial monolayers, Phys. Rev. E 92 (2015) 032729, , https://doi.org/10.1103/PhysRevE.92.032729.
[20] K.D. Schulze, B.A. I, S. Marshall, K.G. Rowe, A.C. Dunn, Real area of contact in a soft transparent interface by particle exclusion microscopy, J. Tribol. 138 (2016), https://doi.org/10.1115/1.4032822 (041404). 6.
[21] R. Benitez, S. Moreno-Flores, V.J. Bolos, J.L. Toca-Herrera, A new automatic contact point detection algorithm for AFM force curves, Microsc. Res. Tech. 76 (8) (2013) 870–876, https://doi.org/10.1002/jemt.22241.
[22] P. Hermanowicz, M. Sarna, K. Burda, H. Gabrys, AtomicJ an open source software for analysis of force curves, Rev. Sci. Instrum. 85 (2014) 063703, , https://doi.org/10.1063/1.4881683.
[23] N. Gavara, R.S. Chadwick, Relationship between cell stiffness and stress fiber amount, assessed by simultaneous atomic force microscopy and live-cell fluorescence imaging, Biomech. Model. Mechanobiol. 15 (3) (2015) 511–523, https://doi.org/10.1007/s10237-015-0706-9.
[24] R. Simic, C.H. Mathis, N.D. Spencer, A two-step method for rate-dependent nano-indentation of hydrogels, Polymer 137 (2018) 276–282, https://doi.org/10.1016/j.polymer.2018.01.017.
[25] M. Garcia, K.D. Schulze, C.S. O'Bryan, T. Bhattacharjee, W.G. Sawyer, T.E. Angelini, Eliminating the surface location from soft matter contact mechanics measurements, Tribology - Materials, Surfaces, and Interfaces 11 (4) (2017), https://doi.org/10.1080/17515831.2017.1397908.
[26] H. Hertz, Ueber die Beruhrung feser elastischer korper, Journal für die reine und angewandte Mathematik 92 (1882) 156–171.
[27] E. Winkler, Die Lehre von der Elasticitaet und Festigkeit, (1868).
[28] J.M. Uruena, A.A. Pitenis, R.M. Nixon, K.D. Schulze, T.E. Angelini, W.G. Sawyer, Mesh size control of polymer fluctuation subrication in gemini hydrogels, Biotribology 1-2 (2015) 24–29, https://doi.org/10.1016/j.biotri.2015.03.001.
[29] A.C. Dunn, J.M. Uruena, Y. Huo, S.S. Perry, T.E. Angelini, W.G. Sawyer, Lubricity of surface hydrogel layers, Tribol. Lett. 49 (2) (2013) 371–378, https://doi.org/10.1007/s11249-012-0076-8.